Supporting Information of

Rhomboid-shaped Organic Host Molecule with Small Binding Space.   Unsymmetrical and Symmetrical Inclusion of Halonium Ions

Yuji Suzaki, Takashi Saito, Tomohito Ide and Kohtaro Osakada*

Chemical Resources Laboratory R1-3, Tokyo Institute of Technology

4259 Nagatsuta, Midoriku, Yokohama 226-8503, Japan.

Fax: +81-45-924-5224; Tel: +81-45-924-5224

E-mail: kosakada@res.titech.ac.jp

.

Computational Details

        Ground state geometry optimization was performed by PBE38[S1] density functional with TZVP (for H, C, N, Cl), LANL2TZ (for Zn, Ag) and LANL08 (for Br) basis sets.　To improve computational speed, the RIJCOSX approximation in combination with TZV/J auxiliary basis set was applied.　The computational method describe above denotes RIJCOSX-PBE38/TZVP in SI, but all PBE38/TZVP (and combination with LANL2TZ/LANL08) computation using approximation was denoted PBE38/TZVP due to simplify in the text.　The PBE38 functional that includes $3/8 = 37.5\%$ Hartree–Fock exact exchange was chosen by results of preliminary calculations (Figure S1). TD-DFT vertical excitation energy was obtained by RIJCOSX-PBE38/TZVP with Tamm−Dancoff approximation (it denotes TDA-RIJCOSX-PBE38/TZVP).　TD-DFT excited state geometry optimization was carried out by TDA-RIJCOSX-PBE38/TZVP level of theory.　Stationary points of both ground and excited state were characterized by Hessian calculation.　Potential energy curve was obtained by relax potential energy surface scan calculation that N–N distance is constrained at RIJCOSX-PBE38/TZVP level of theory.　Excitation and fluorescent wavelength in solution were also consider single point TDA-RIJCOSX-PBE38/TZVP calculation with COSMO solvation model. All calculations were performed by ORCA 2.9.1[S2].　The plots (isosurface = 0.02) of the frontier orbitals were drawn by VESTA 3.1.4[S3].

References

(S1) Grimme, J. Antony, S. Ehrlich and H. Krieg, *J. Chem. Phys.* **2010**, *132*, 154104.

(S2) F. Neese, *WIREs Comput. Mol. Sci.* **2012**, *2*, 73.

(S3) K. Momma and F. Izumi, *J. Appl. Crystallogr.* **2011**, *44*, 1272.

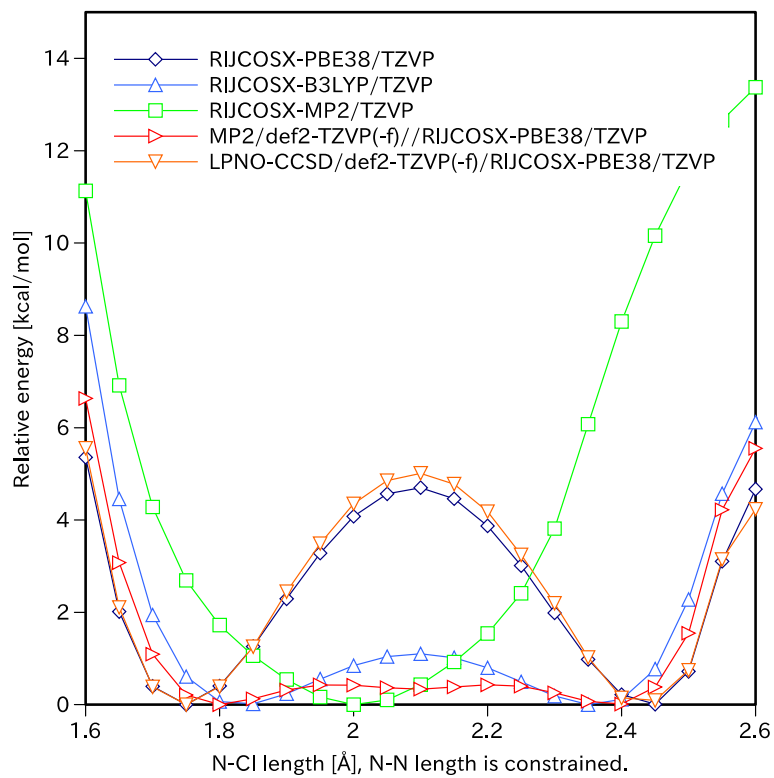(S4) F. Neese, A. Hansen and D. G. Liakos, *J. Chem. Phys.* **2009**, *131*, 064103.

Figure S1. Potential energy curves (N–Cl length) of selected preliminary calculation methods. RIJCOSX-PBE38/TZVP affords comparable result to the most accurate method in the preliminary calculations, LPNO-CCSD[S4]/def2-TZVP(-f)//RIJCOSX-PBE38/TZVP.
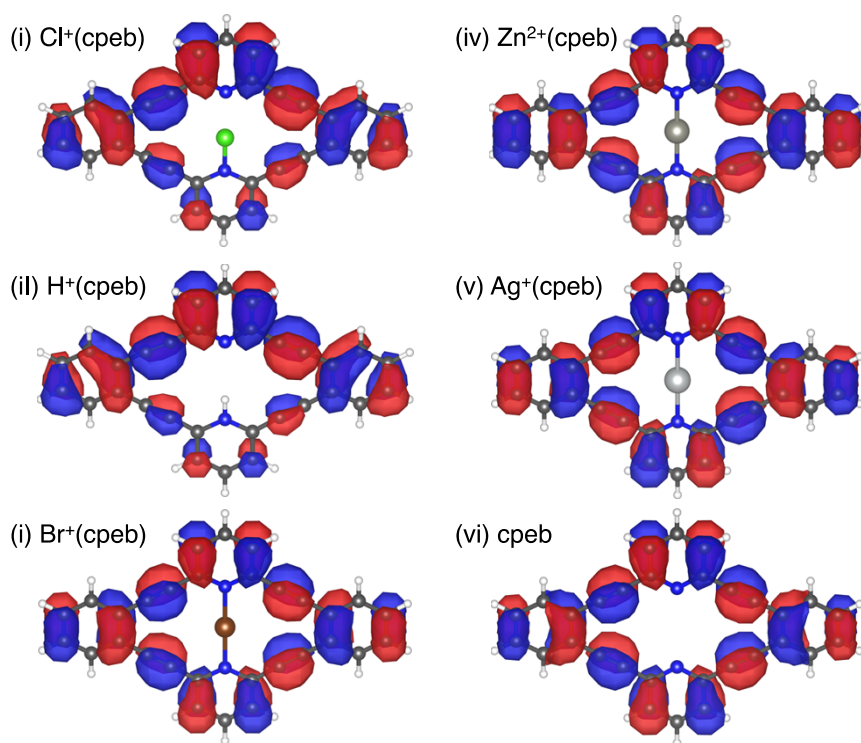
Figure S2. Calculated HOMO (highest occupied molecular orbital) of (i) Cl⁺(cpeb), (ii) H⁺(cpeb), (iii) Br⁺(cpeb), (iv) Zn²⁺(cpeb), (v) Ag⁺(cpeb) and (vi) cpeb.
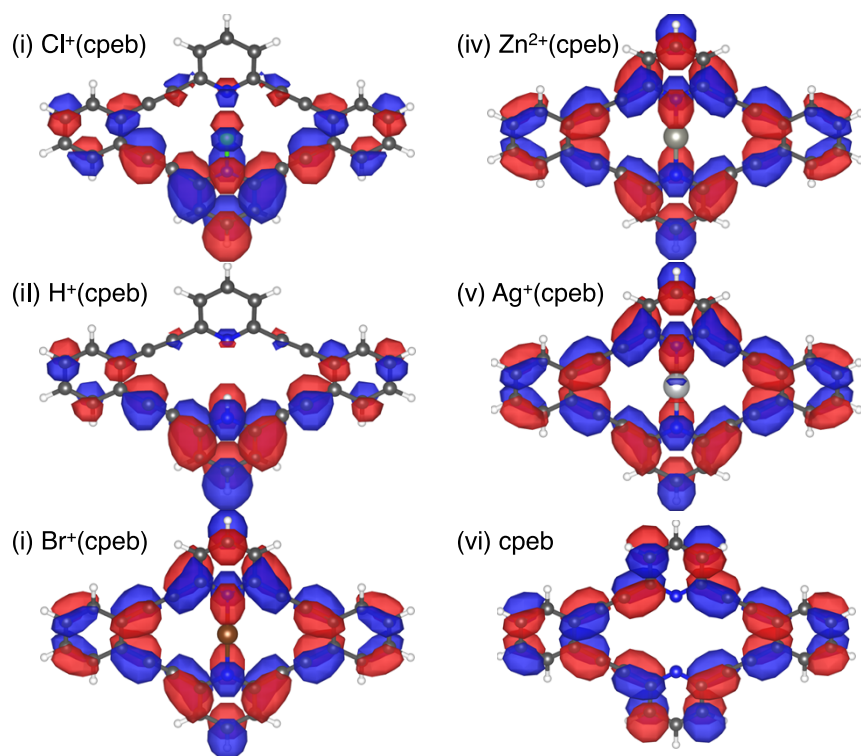
Figure S3. Calculated LUMO (lowest unoccupied molecular orbital) of (i) Cl⁺(cpeb), (ii) H⁺(cpeb), (iii) Br⁺(cpeb), (iv) Zn²⁺(cpeb), (v) Ag⁺(cpeb) and (vi) cpeb.
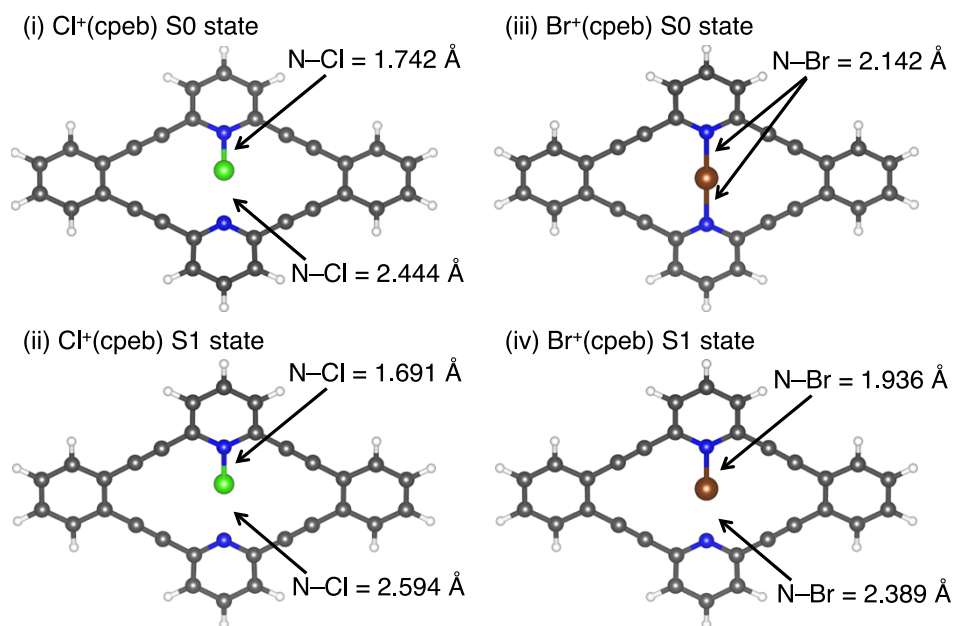
Figure S4. N–X (X = Cl⁺, Br⁺) length of (i) Cl⁺(cpeb) S0 state, (ii) Br⁺(cpeb) S0 state, (iii) Cl⁺(cpeb) S1 state and (iv) Br⁺(cpeb) S1 state.

Table S1. Calculated absorption wavelength of the compounds in gas phase.

	S1/nm	f(S1)	S2/nm	f(S2)	S3/nm	f(S3)
cepb	340.0	0.0000	304.7	0.8850	285.8	0.0000
H^+(cpeb)	464.7	0.0632	356.7	0.3218	353.0	0.5103
Cl^+(cpeb)	440.4	0.0579	347.6	0.3126	342.0	0.5265
Ag^+(cpeb)	367.9	0.0000	307.4	0.8061	304.2	0.6563
Br^+(cpeb)	392.0	0.0000	323.0	0.4666	309.6	0.7807
Zn^{2+}(cpeb)	424.1	0.0000	378.2	0.0000	351.3	0.4494

Table S2. Calculated absorption wavelength of the compounds in CH_2Cl_2 (gas phase geometry).

	S1/nm	f(S1)	S2/nm	f(S2)	S3/nm	f(S3)
cepb	342.5	0.0000	301.8	0.8822	282.9	0.3410
H^+(cpeb)	436.2	0.0788	342.2	0.4629	345.0	0.4770
Cl^+(cpeb)	429.9	0.0627	339.0	0.5390	342.3	0.3928
Ag^+(cpeb)	365.3	0.0000	304.8	0.8031	300.9	0.5332
Br^+(cpeb)	388.4	0.0000	319.0	0.4677	308.2	0.7538
Zn^{2+}(cpeb)	407.6	0.0000	332.2	0.3906	345.3	0.0000

Table S3. Calculated fluorescent wavelength of the compounds in gas phase.

	S0←S1/nm	f(S0←S1)
cepb	378.0	0.0000
H^+(cpeb)	521.2	0.0371
Cl^+(cpeb)	504.1	0.3646
Ag^+(cpeb)	411.8	0.0000
Br^+(cpeb)	457.7	0.0282
Zn^{2+}(cpeb)	481.3	0.0000

Table S4. Calculated fluorescent wavelength of the compounds in CH_2Cl_2 (gas phase geometry).

	S0←S1/nm	f(S0←S1)
cepb	382.1	0.0000
H^+(cpeb)	489.3	0.0000
Cl^+(cpeb)	491.5	0.0394
Ag^+(cpeb)	409.9	0.0000
Br^+(cpeb)	453.3	0.0254
Zn^{2+}(cpeb)	463.6	0.0000
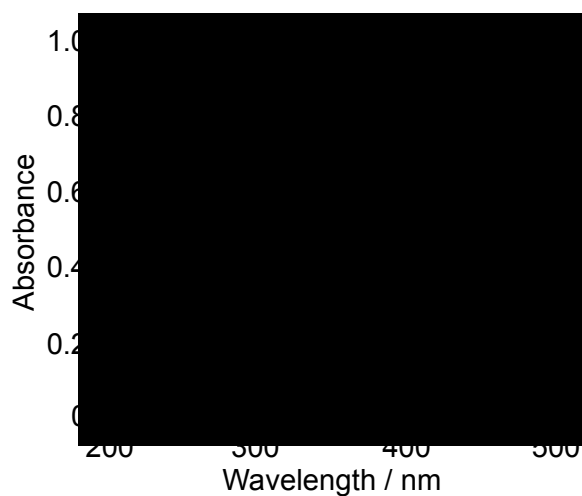
Figure S5.   UV-spectra of Ag(cpeb)OTf (r.t., 1.0×10^{-2} mM, generated in situ by reaction of cpeb and AgOTf in CH_2Cl_2 (10 mL)) before and after addition of Cl_2. Cl_2 gas, used in the measurement was generated by mixing 1 M HCl(aq) (10 mL) and 1 M NaOCl (5.0 mL)

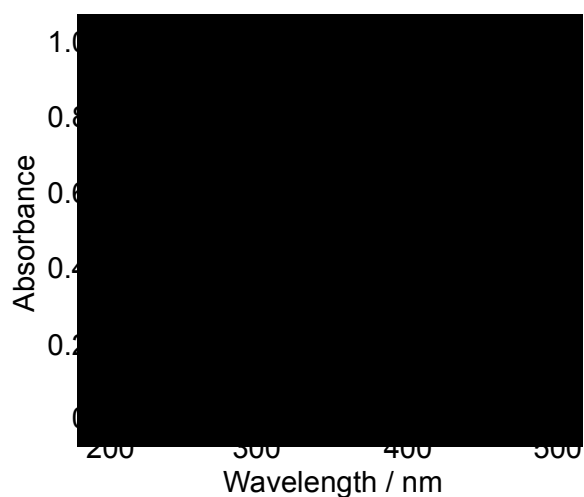Figure S6.   Change in UV-vis spectra of Ag(cpeb)OTf (CH_2Cl_2, r.t., 1.0×10^{-2} mM, generated in situ by reaction of cpeb and AgOTf) by addition of Br_2 ($\sim2.0\times10^{-2}$ mM).
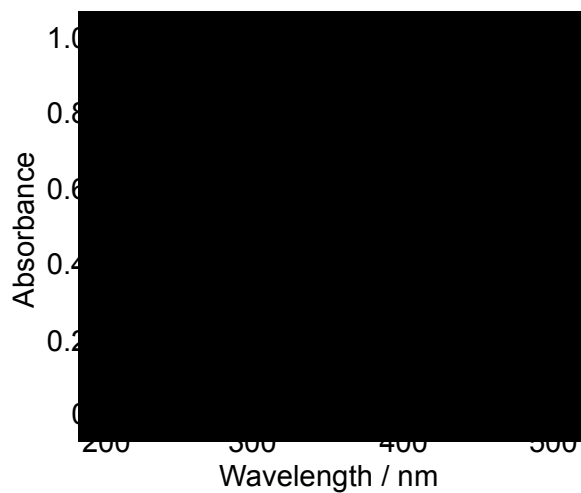
Figure S7. Change in UV-vis spectra of cpeb (CH$_2$Cl$_2$, r.t., 1.0×10^{-2} mM) by addition of AgOTf ($\sim 2.0 \times 10^{-2}$ mM).
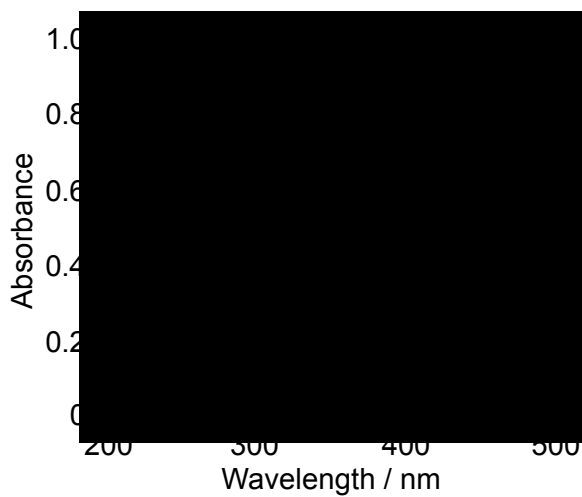
Figure S8. Change in UV-vis spectra of cpeb (CH$_2$Cl$_2$, r.t., 1.0×10^{-2} mM) by addition of Pd(OCOCF$_3$)$_2$ ($\sim 4.0 \times 10^{-2}$ mM).

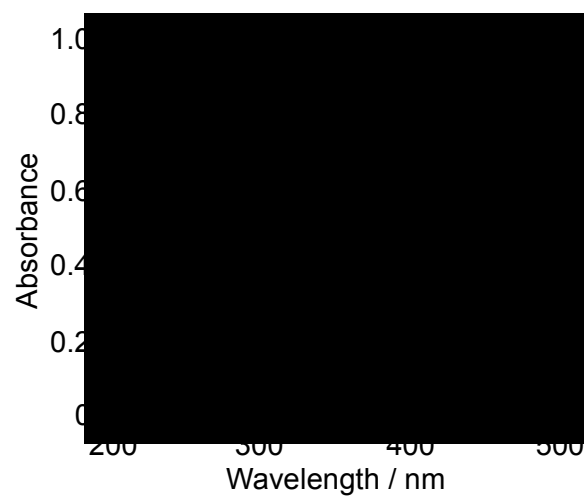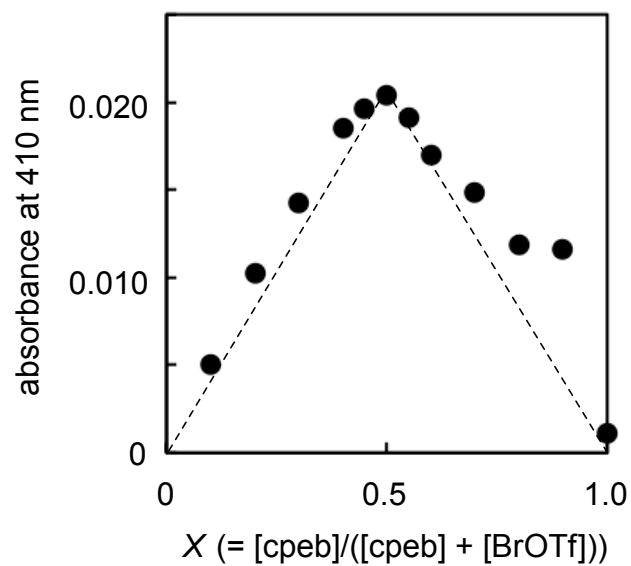Figure S9.　Change in UV-vis spectra of cpeb (CH$_2$Cl$_2$, r.t., 1.0×10^{-2} mM) by addition of Zn(OTf)$_2$ (~2.0×10^{-2} mM).
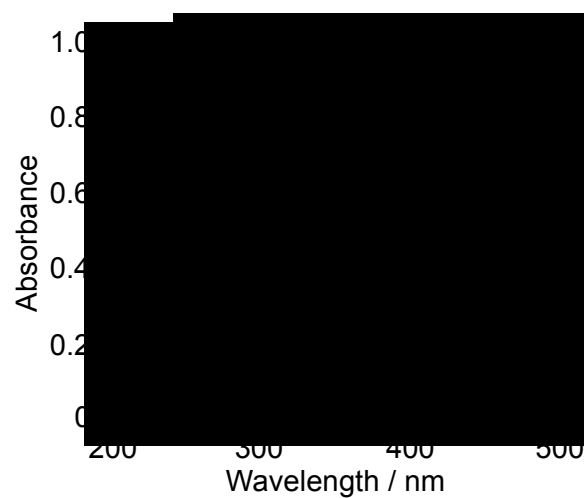
Figure S10.　Change in UV-vis spectra of cpeb (CH$_2$Cl$_2$, r.t., 1.0×10^{-2} mM) by addition of TFA (~10 mM).

Figure S11.　Job's plot of Br(cpeb)OTf obtained from absorption spectra (CH_2Cl_2, 25 $^{\circ}C$, $\lambda_{abs} = 410$ nm, [cpeb]+[BrOTf] = 1.0×10^{-2} mM).
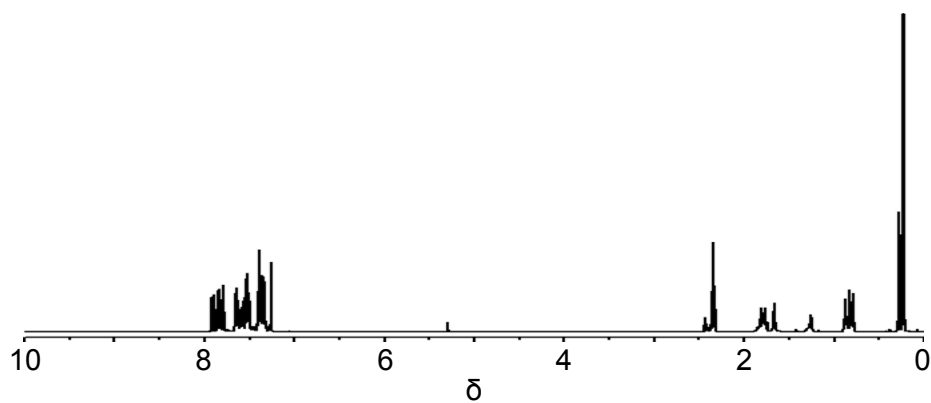
Figure S12. ^{1}H NMR spectrum of **3** (CDCl$_3$, 300 MHz, r.t.)
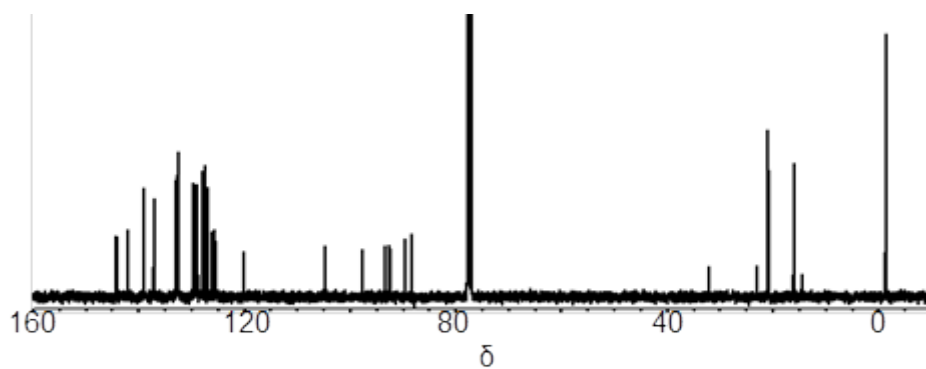

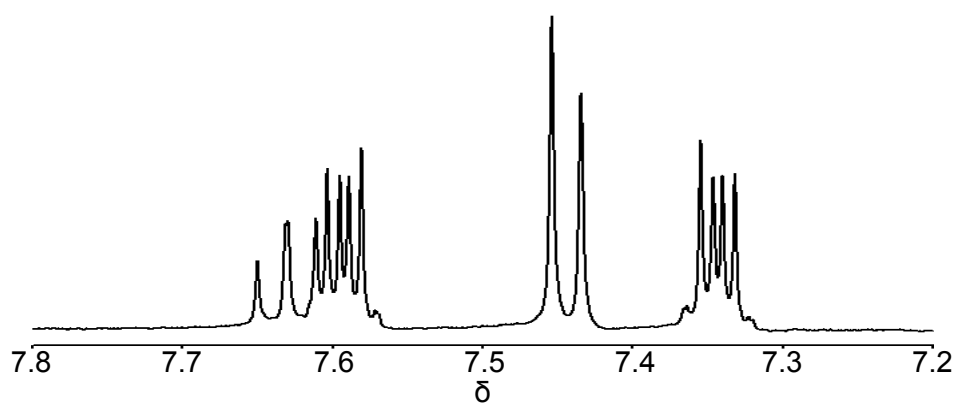Figure S13. $^{13}C\{^{1}H\}$ NMR spectrum of **3** (CDCl$_3$, 100 MHz, r.t.)

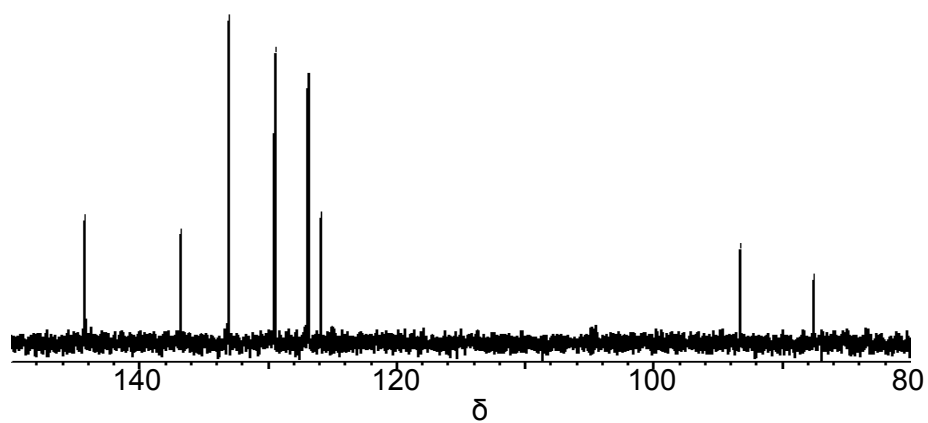Figure S14. ^{1}H NMR spectrum of cpeb (CD$_2$Cl$_2$, 300 MHz, r.t.)

Figure S15. ^{13}C{^{1}H} NMR spectrum of cpeb (CD$_2$Cl$_2$, 100 MHz, r.t.)